5th ECPMG Delft · 2024

Proceedings of the 5th ECPMG 2024
5th European Conference on Physical Modelling in Geotechnics
2-4 October 2024, Delft, the Netherlands

Dynamic centrifuge modelling of the effect of a superstructure on the dynamic response of rigid inclusions

C. Nohra, C. Soriano-Camelo, S. Escoffier, Z. Li, L. Thorel
Univ Gustave Eiffel, GERS-CG, F-44344 Bouguenais, France, charbel.nohra@univ-eiffel.fr, cristian.soriano-camelo@univ-eiffel.fr, sandra.escoffier@univ-eiffel.fr, zheng.li@univ-eiffel.fr, luc.thorel@univ-eiffel.fr

ABSTRACT: This paper discusses the dynamic efforts developed in a rigid inclusions (RI) reinforcement system supporting a slender structure by means of two dynamic centrifuge tests performed at Gustave Eiffel University, France. The two small scale models are constituted of a similar soil column reinforced by seven rigid inclusions. One of the tests involved the placement of a slender structure on top of the soil mass. The tests are conducted at a macro-gravity of 50g and both configurations are subjected to the same predetermined sequence of seismic events constituted of sinusoidal motions and multi-frequency earthquakes with different peak ground accelerations. Results are presented in terms of maximum dynamic bending moments, axial forces recorded in the instrumented RI and lateral displacements. Results reveal that the placement of the superstructure exerts little impact on RI bending moments and lateral displacements but induces larger axial force.

1 INTRODUCTION

The rigid inclusions (RI) reinforcement system involves installing vertical columns in a layer of soft soil and placing a granular layer called Load Transfer Platform (LTP) between the inclusion heads and the structure or foundation. Contrary to pile foundations where the entire structure load is supported by the piles, the RI systems divides the loads between the RI and the soft soil. As less loads are supported by the RI, the decrease of the demand induces an economical design (ASIRI National Project, 2012). Reinforcement by RI has been implemented in various works, such as the Rio-Antirrio bridge (Pecker, 2004, 2006) and the Izmit Bay bridge (Steenfelt et *al*., 2015). It has been shown that higher loads can be supported when rigid inclusions are used.

The advantage of RIs reinforced systems under dynamic loads has become an increasingly popular concept for researchers. Ko et *al.*, (2019) evaluated the effect of RI location and material on the developed bending moments using dynamic centrifuge tests. It was found out that the dynamic bending moments in the RIs are governed by the soil, rather than by the matrials of the RIs. In addition, the edge piles support larger moments than the middle pile due to the shielding effect (Yang et *al*., 2022). Li et *al.*, (2024) performed 1g shaking table tests to investigate the effect of the LTP thickness and material on RI moments and it has been shown that higher thickness and rounded particles reduced the bending moments in the RIs. The centrifuge tests of Baziar et *al.* (2018) showed that the studied structure types had no influence on the bending moments in the piles. Contradictory, the numerical analysis of Jiménez and Dias (2022) showed that the maximum shear forces and bending moments in piles depend on the dynamic properties of the superstructure. Finally, the site model experiment of Sekiguchi et *al.* (2015) showed that the presence of a LTP leads to an almost complete reduction of the inertial load transmission from the superstructure to the RIs under which very little bending moments were recorded at the heads.

This paper investigates how a slender structure on the LTP affects the axial forces, bending moment in and the deformations of the RI. The analysis is based on the comparison of two centrifuge tests performed under a microgravity of 50*g* on a soil mass reinforced by RI. In the first test, test C-RI, no superstructure was supported while, in the second test, test C-S-RI, a rigid slender structure was placed on the LTP. Figure 1 shows cross sections of both centrifuge tests.

2 METHODOLOGY

This section describes the methodology followed for the preparation of the soil, as well as the properties of the rigid elements used (RI and Structure) and the characteristics of the input motions applied during the tests. In this part, the model scale values are presented followed by the prototype values between parenthesis.

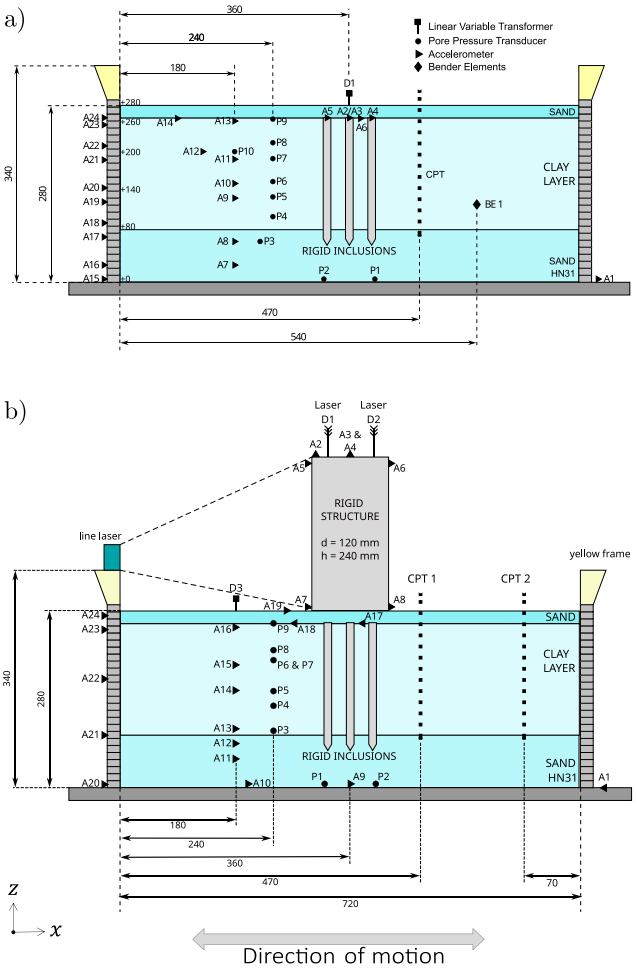

Figure 1. Elevation view of the model containers with the distribution of instruments (model scale in mm): a) C-RI; b) C-S-RI

2.1 Soil mass preparation

The same soil column was considered for the two tests. The soil column was reconstituted in a Laminar Shear Beam (LSB) container in order to minimize the boundary effects (Lee et *al.*, 2012). The LSB is constituted by an assembly of frames, separated by rollers to minimize the shear resistance and the frame mass is minimized to reduce as far as possible the inertial forces induced by the frame acceleration during the shaking event. The top yellow frame is a frame with smaller mass and is the origins for all vertical dimensions. In addition, lateral reinforcements avoid excessive ovalisation to maintain K_0 condition.

A three-layer soil model was considered: the first layer was constituted of 8 cm (4 m) of dense Hostun sand HN31 with a relative density D_r of 80% installed using air pluviation; the second layer was 18 cm (9 m) of overconsolidated clay-sand mix; and above that, 2 cm (1 m) of well graded sand mix was installed. The soft layer was constituted of 80% kaolin clay and 20% Fontainebleau sand. Kaolin clay was best used since it has a relatively higher permeability than other clay making the consolidation time shorter (Pérez-Herreros, 2020). Note that the soft layer was overconsolidated under a consolidation pressure of 120 kPa to obtain an average undrained shear strength S_u of 20 kPa. The experimental methodology was presented in detail by Nohra et *al.*, (2024).

After the installation of each layer, sensors such as 1D accelerometers (frequency range: 1 Hz to 20 kHz), noted as "A", Pore Pressure Transducers, noted as "P" as well as Bender Elements noted as "BE", that are used for the determination of the shear wave velocity V_s are placed into the soil (Figure 1). The instruments "A' and "P" are placed in the symmetry plane while the "BE" correspond to a pair of sensors positioned at the same depth and separated by a distance of 100 mm in the (x,y) plane.

2.2 Rigid Inclusions and Superstructure

Before the installation of the LTP, seven RI were installed in the cohesive layer at 1*g* using a vertical actuator that pushed them at a velocity of 0.1 mm/s. The model RI are aluminum tubular RI with a length of 20 cm (10 m) and an external diameter of 12 mm (60 cm). They have a bending stiffness (*EI*) of 39 N.m² (244 MN.m²) and a compression stiffness (*EA*) of 2.56 MN (6.39 GN). Figure 2 shows a schematic representation of the RI with the locations of instrumentation. Four of the seven RIs were instrumented by six stain gauges: four gauges (locations 2, 3, 4 and 6) were calibrated to measure the bending moments, and the other two (locations 1 and 5) the axial forces.

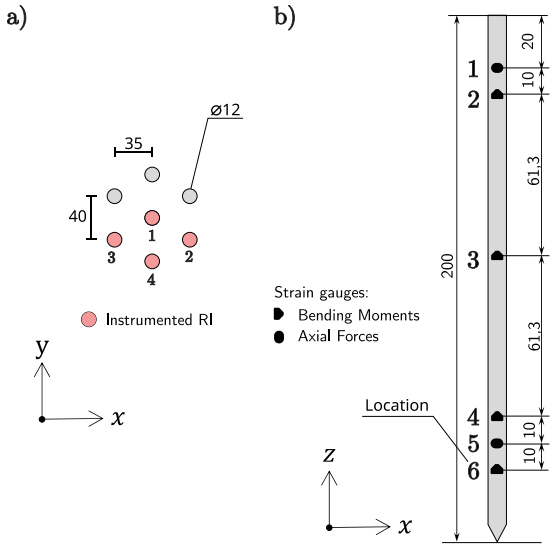

Figure 2. a) Distribution of RI and; b) location of strain gauges (model scale in mm)

The tested superstructure is a hollow cylinder having a height of 24 cm (12 m) and a diameter of 12 cm (6 m). It weighs approximately 1.3 kg (162 tonnes) and has a slenderness ratio of 1.5. The structure is instrumented by four horizontal accelerometers installed on the structure's cap and four vertical accelerometers at the top. Two laser sensors were installed at the top of the structure in order to monitor its settlement and rotations. Finally, a linear laser was also installed laterally to monitor the lateral displacement of the structure. Impact hammer tests were conducted to determine the fixed base natural frequency of the structure and the RI. For this purpose, accelerometers were glued on top of a rigid surface and were subjected to a pulse using a hammer in the direction of the accelerometers. It was found that the fixed base natural frequency of the RI and structure are respectively 190 Hz (3.8 Hz) and 390 Hz (7.8 Hz). It is important to mention that the natural frequency of the structure is larger than most of the frequency content of the ground motions, meaning that it can be considered as a rigid structure.

2.3 Input motions

Dynamic input motions were applied by means of the shaking simulator of the Gustave Eiffel University (Chazelas et *al.*, 2008). A sequence of twenty ground motions was applied on both models. Due to inaccuracies in the shaking table, it is important to verify that the input motions between the two tests are similar. Therefore, the differences between the recorded base shaking are first analysed and compared in terms of PGA, PGV and PGD as well as the difference between both tests for all ground motions (using accelerometer A1). Some large differences in PGA (signal #3, #13 and #20) are probably due to experimental inaccuracy of the shaking table that can generate some high frequencies noise. The smallest difference is observed for PGD. Passing from acceleration to displacement requires integration with respect to time, which is responsible of the filtering of high frequency noises recorded in the acceleration. Overall, the difference in terms of input motions in not significant, indicating that the results obtained are fairly comparable.

3 RESULTS

Results are discussed in terms of inertial efforts developed (bending moments and axial forces) as well as the lateral movement of the piles head. All results are presented in prototype scale.

3.1 Bending Moments

The effect of the superstructure on the RI's response is investigated by comparing the evolution of bending moment over the sequence of ground motions. To do so, the maximum dynamic bending moments for each ground motion was determined for the four instrumented RI. At first, the comparison is conducted for all RI at all strain gauges. Figure 3 shows the evolution of M_{max} for RI 2 at all moment strain gauges across the ground motions sequence. Except some differences especially during GM #3, #4 and #5, $M_{\max}$ are close between the two tests for RI 2.

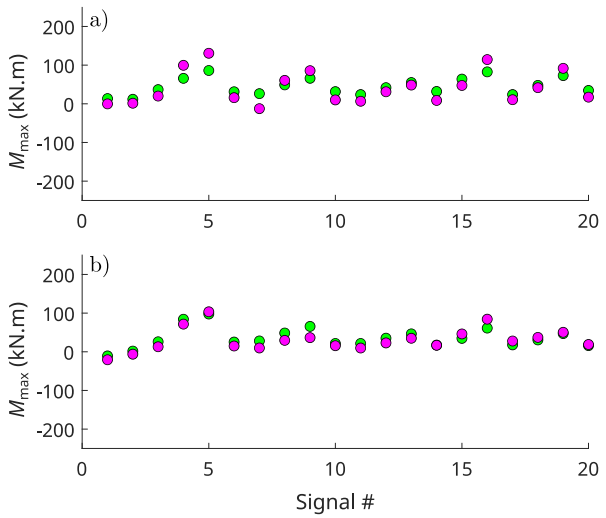

Figure 3. Evolution of M_{max} for RI 3 at strain gauges: a) location 2 and; b) location 4 across the ground motions sequence.

To take into account the remaining RI, $M_{\max}$ were averaged between the four instrumented RI and the evolution obtained is shown in Figure 4 at the location 3. Results show that the values and trend of $M_{\max}$ of tests C-RI and C-S-RI are similar. This finding suggests that $M_{\max}$ is less influenced by the structure's inertia (inertial interaction) than kinematic effects. The maximum bending moment corresponds to the ground motion *Sine 1Hz 0.25g*, with a bending moment of 380 kN.m at location 3.

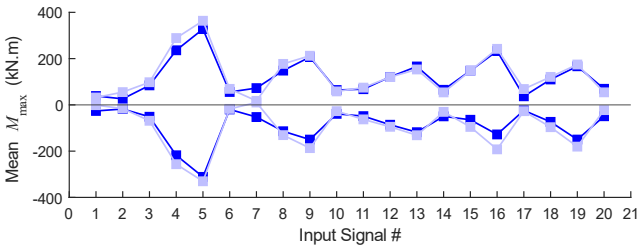

Figure 4. Mean maximum bending moment during all ground motions in both tests at location 3

Table 1. Input motions order, PGA, PGV and PGD and percent difference during both tests

#	Signal	PGA (g)			PGV (g)			PGD (g)		
		C-RI	C-S-RI	Diff (%)	C-RI	C-S-RI	Diff (%)	C-RI	C-S-RI	Diff (%)
1	Landers 0.05g	0.076	0.064	-15.70	3.52	2.63	-25.23	0.837	0.801	-4.35
2	Northridge 0.05g	0.066	0.059	-10.99	3.82	3.13	-18.15	0.451	0.404	-10.35
3	Sine 1 Hz 0.05g	0.131	0.084	-35.60	9.76	8.18	-16.23	1.498	1.329	-11.26
4	Sine 1 Hz 0.15g	0.293	0.250	-14.55	27.87	24.23	-13.05	4.420	3.836	-13.22
5	Sine 1 Hz 0.25g	0.424	0.415	-2.19	45.08	38.03	-15.63	7.125	6.182	-13.24
6	Landers 0.05g	0.066	0.073	11.68	4.50	3.65	-18.94	0.690	0.651	-5.69
7	Sine 1.8 Hz 0.05g	0.090	0.070	-22.39	4.94	4,33	-12.37	0.431	0,375	-12,99
8	Sine 1.8 Hz 0.15g	0.254	0.214	-15.82	15.41	12.54	-18.65	1.343	1.144	-14.83
9	Sine 1.8 Hz 0.25g	0.429	0.342	-20.29	25.49	21.41	-15.99	2.249	1.945	-13.49
10	Landers 0.05g	0.080	0.071	-10.48	4.35	3.47	-20.17	0.706	0.694	-1.59
11	Sine 2.4 Hz 0.05g	0.094	0.084	-10.15	5.01	3.88	-22.54	0.307	0.271	-11.58
12	Sine 2.4 Hz 0.15g	0.246	0.186	-24.36	12.07	9.34	-22.65	0.759	0.628	-17.28
13	Sine 2.4 Hz 0.25g	0.424	0.282	-33.43	20.33	15.37	-24.41	1.272	1.044	-17.93
14	Landers 0.05g	0.080	0.066	-17.03	4.31	3.19	-26.04	0.747	0.699	-6.39
15	Landers 0.15g	0.166	0.119	-28.02	11.91	9.99	-16.16	1.985	1.695	-14.61
16	Landers 0.30g	0.326	0.315	-3.35	22.30	19.24	-13.73	3.922	3.464	-11.67
17	Northridge 0.05g	0.069	0.060	-13.25	4.35	3.77	-13.22	0.492	0.438	-10.90
18	Northridge 0.15g	0.196	0.187	-4.44	10.75	8.80	-18.14	1.405	1.246	-11.33
19	Northridge 0.30g	0.426	0.365	-14.30	19.66	16.57	-15.74	2.793	2.381	-14.77
20	Landers 0.05g	0.080	0.046	-42.95	4.44	3.28	-26.04	0.705	0.670	-4.92

Analytical calculations for an isolated RI showed that the ultimate moment M_{ult} of the RI is 2690 kN.m and the allowable moment is 25% of the M_{ult}, thus 672 kN.m, larger than the M_{max} obtained. It is therefore verified that the RI are not plastified under severe ground motions.

3.2 Axial forces

Although bending moments in RI are not influenced by the structure, the axial forces differ significantly due the additional weight induced by the presence of the superstructure. Analysis consisted of determining the percent change in axial force ΔF with respect to the axial force recorded directly prior to the application of the first ground motion. Evolution of ΔF is represented in Figure 4 for the strain gauges near the head of the RI (z/D = 1.7). Due to a disfunction of the strain gauge of RI 4, the results regarding C-RI (Figure 5a) show only those of RI 1, 2 and 3. Each abrupt change in axial force corresponds to one ground motion and the duration between two successive ground motions is approximately five minutes at the model scale that corresponds to 4 hours in prototype. Compression is represented as positive and traction as negative. It is observed that during each ground motion, compression drops in the RI due to the pore pressure build up that decrease lateral effective stresses on the RI.

For the case without a structure (Figure 5a), an almost similar trend is observed for the three RI. The overall trend shows that RI 1 (centre) witnessed the smallest total ΔF among the three (65%). Also, except for the larger drops observed for RI 3 during two of the early strong sines (at t = 6.2 days and t = 6.6 days), the values are almost similar to RI 2 over the remaining ground motions with total ΔF of 76% for RI 2 and 82% for RI 3. This shows that the response of the RI in terms of axial forces is almost similar without the structure.

The results with the structure (Figure 5b) show a different response of the RI. Larger drops are observed for the lateral RI (2 and 3) than the centre RI (1 and 4) during the first two motions (t = 7.1 days and t = 7.3 days). The drops values increase for RI 1, 2 and 4 until ΔF of 60%, 73% and 51% after the fifth motion (*Sine 1 Hz 0.25g* at t = 7.8 days) after which the drops for these three RI are always smaller. It can be also seen that the drop after each ground motion is followed by a recuperation phase, during which the axial forces increase progressively. Unfortunattelly, the recordings of the pore pressure inside the clay-sand layer are not sufficently reliable to validate this assumption. Figure 4a shows that prior to *Sine 1 Hz 0.25g*, the recuperation

is almost similar for RI 1, 2 and 4 and larger for RI 3. This may be due to the rotation of the building towards RI 3 inducing larger vertical forces applied thus larger water dissipation. After signal #5 the recuperation is different between the RI: RI 3 and 4 witnessed large recuperations, whereas RI 1 and 2 witnessed small and no recuperations respectively. This has led to the progressive increase of axial forces in RI 3 and decrease in RI 2. Also, it can be seen that the recuperation rate is largest for RI 3 and decrease progressively for RI 4, 1 and 2 (see the tangent lines at t = 8.5 days).

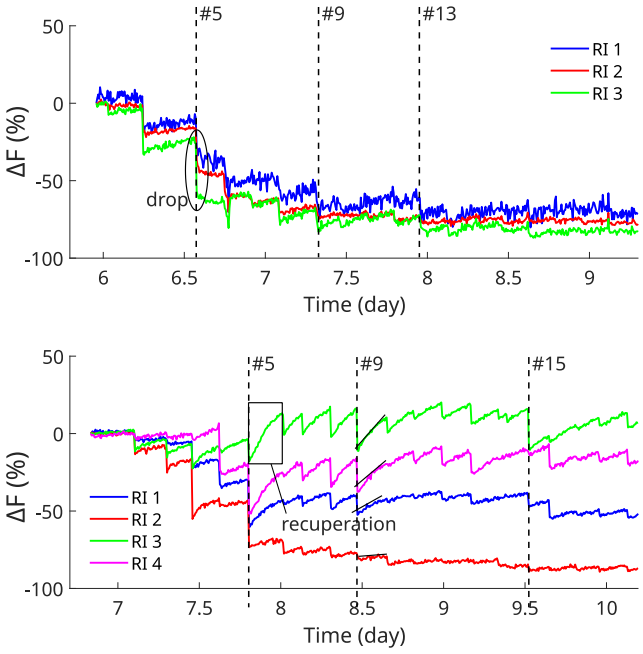

Figure 5. Evolution of axial forces during centrifuge test.: a) C-RI; b) C-S-RI

This behaviour can be explained by the direction of the rotation of the building. During the sequence of ground motions, residual rotations towards RI 3 are observed, thus RI 3 witnessed the largest external vertical force among the four RI, which explain the larger developed internal axial forces. It can also be noted that the total drop of RI 2 is 87%, value close to the total drop for C-RI, meaning that RI 2 behaved almost similarly in both tests. Also, results may indicate that the larger the vertical force on the RI head, the larger the recuperation rate.

The structure's rotation can also be observed by representing the evolution of the axial forces during one ground motion. Figure 6 shows the results obtained during signal #5. Similar to Figure 5, the axial forces in the central RI are similar whereas the forces are greater in RI 3 and smaller in RI 2. Also, it is observed that the axial forces in RI 2 ad RI 3 are oscillating at opposite phases, reflecting the structure's rotations.

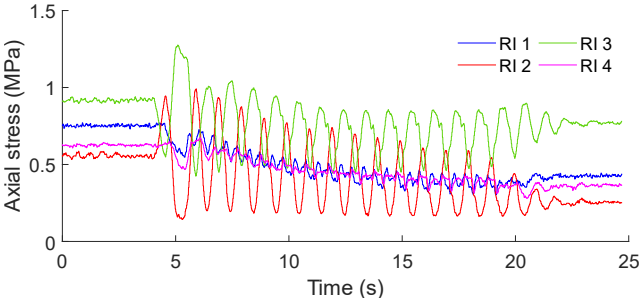

Figure 6. Axial stresses during Sine 1Hz 0.25g (signal #5)

3.3 Head lateral displacement

Using the bending moments profile, it is possible to deduce the lateral displacement of the piles using the equation

$$\frac{d^2 Y}{dz^2} = E\,I\,M(z) \qquad (1)$$

Where Y is the lateral displacement, z is the vertical ordinate along the RI. For the integration, it was assumed that the RI are rigidly anchored at the base, thus the limit conditions adopted were $Y'(0) = Y(0) = 0$. Figure 7 represents the time histories of the lateral displacement at the head of the four RI obtained during *Northridge 0.3g* for both tests. Results show that the displacements of the four inclusions are almost in phase since RI 2 is slightly late, thus the superstructure's additional weight has no effect on the motion of the RI. Also, the displacement of RI 3 and RI 2 are smaller than RI 1 and RI 4.

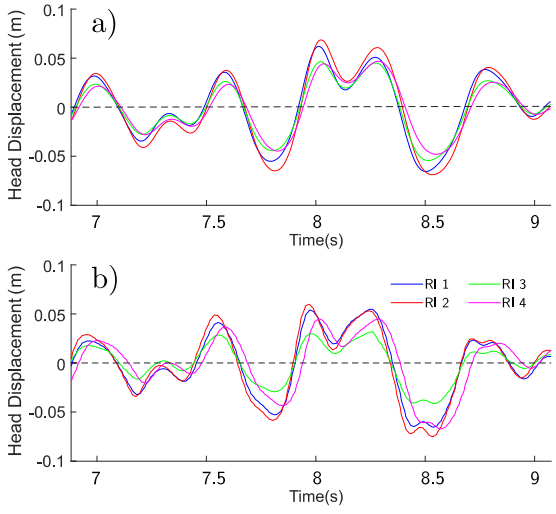

Figure 7. Lateral head displacement of the RI: a) C-S-RI; b) C-RI

This may be due to the screen effect between RI 2 and 3. Also, comparing both tests, similar values of lateral displacement were observed, thus the superstructure has no effect on the dynamic movements of the RI.

4 CONCLUSIONS

In this paper, two dynamic centrifuge tests were presented and discussed in order to study the effect of a superstructure on the response of Rigid Inclusions. The two tests, denoted respectively as C-RI and C-S-RI are constituted of a similar reinforced soil mass supporting a slender structure in the case of the latter test. A sequence of twenty ground motions was applied on the models and the results for the considered configuration are summarized as follows:

- Maximum bending moment and lateral displacement of the RI are not affected by the presence of the superstructure.
- Axial forces are larger when the superstructure is installed and especially in the RI towards which the structure rotates after each earthquake.
- Higher vertical forces on the RI head induced recuperation of the compression forces after the ground motion.
- Lateral RI experience larger and opposing phases cycles of dynamic axial forces due to the rotation of the superstructure.

ACKNOWLEDGEMENTS

The authors want to thank the French National Research Agency for funding the ASIRIplus_SDS project (ANR-19-C22-0015), as well as the Pays de la Loire region and the Gustave Eiffel University for the Ph.D grant. Special thanks to the GERS-CG technical team as well.

REFERENCES

ASIRI National Project (2012). *Recommendations for the Design, Construction and Control of Rigid Inclusion Ground Improvements*. Retrieved from Presses des Ponts, Paris (in French).

Baziar, M. H., Rafiee, F., Lee, C. J., & Saeedi Azizkandi, A. (2018). Effect of superstructure on the dynamic response of nonconnected piled raft foundation using centrifuge modelling. *International Journal of Geomechanics*, *18*(10), 04018126. https://doi.org/10.1061/(ASCE)GM.1943-5622.0001263

Chazelas, J. L., Escoffier, S., Garnier, J., Thorel, L., & Rault, G. (2008). Original technologies for proven performances for the new LCPC earthquake simulator. *Bulletin of earthquake engineering*, *6*, 723-728. https://doi.org/10.1007/s10518-008-9096-z

Jiménez, G. A. L., & Dias, D. (2022). Dynamic soil–structure interaction effects in buildings founded on vertical reinforcement elements. *CivilEng*, *3*(3), 573-593. https://doi.org/10.3390/civileng3030034

Ko, K. W., Park, H. J., Ha, J. G., Jin, S., Song, Y. H., Song, M. J., & Kim, D. S. (2019). Evaluation of dynamic bending moment of disconnected piled raft via centrifuge tests. *Canadian Geotechnical Journal*, *56*(12), 1917-1928. https://doi.org/10.1139/cgj-2018-0248

Lee, C. J., Wei, Y. C., & Kuo, Y. C. (2012). Boundary effects of a laminar container in centrifuge shaking table tests. *Soil Dynamics and Earthquake Engineering*, *34*(1), 37-51. https://doi.org/10.1016/j.soildyn.2011.10.011

Li, Z., El Naggar, M. H., Dai, G., Liu, H., Luan, Y., & Gong, W. (2024). Seismic isolation effect of unconnected piles-caisson foundation: Large-scale shake table tests. *Soil Dynamics and Earthquake Engineering*, *176*, 108304. https://doi.org/10.1016/j.soildyn.2023.108304

Nohra, C., Soriano-Camelo, C., Escoffier, S., Li, Z., Thorel, L. (2024). Experimental study of the kinematic interaction between a cohesive soil and a group of rigid inclusions through dynamic centrifuge tests. *8th International Conference of Earthquake and Geotechnical Engineering*, Osaka, Japan.

Pecker, A. (2004). Design and construction of the Rion Antirion Bridge. In *Geotechnical engineering for transportation projects* (pp. 216-240). https://doi.org/10.1061/40744(154)7

Pecker, A. (2006). Enhanced seismic design of shallow foundations: example of the Rion Antirion bridge. *4th Athenian lecture on Geotechnical Engineering*, 1.

Pérez-Herreros, J. (2020). *Dynamic soil-structure interaction of pile foundations: experimental and numerical study.* Doctoral dissertation, École centrale de Nantes.

Sekiguchi, T., Nakai, S., Yamamoto, M., Fukutake, K., & Taji, Y. (2015). Evaluation of seismic behaviour of the insulated pile foundation based on site model experiment. *10th Pacific Conference on Earthquake Engineering*, Sydney, Australia

Steenfelt, J. S., Foged, B., & Augustesen, A. H. (2015). Izmit Bay bridge geotechnical challenges and innovative solutions. *International Journal of Bridge Engineering*, *3*(3), 53-68.

Yang, Y., Fan, H., Cheng, Y. P., Gong, W., Dai, G., Liang, F., & Jia, Y. (2022). Seismic response of nuclear power station with disconnected pile-raft foundation using dynamic centrifuge tests. Journal of Cleaner Production, 379, 134572. https://doi.org/10.1016/j.jclepro.2022.134572